Multi-sensor placement to exploit complementary properties of diverse sonar waveforms

Doug Grimmett
NATO Undersea Research Center (NURC)
Viale S. Bartolomeo 400, La Spezia, Italy, 19138

This work was conducted while Mr. Grimmett was employed by NATO. He is currently employed by SPAWAR Systems Center San Diego
grimmett@spawar.navy.mil

Abstract - *Distributed multistatic active sonar systems have the potential to greatly improve surveillance capability against threat submarines. The geometric diversity of such systems provides an increased number of complementary detection opportunities to counter the underwater threat. The utilization of both Doppler sensitive and insensitive waveforms within such a multistatic network further improves the detection diversity and provides a more robust surveillance capability. This paper describes the issues relevant to achieve this detection diversity, and shows the potential improvements of this approach. A simplified sonar signal excess model is described, which provides a capability to evaluate distributed sensor placements using both waveform types.*

Keywords: ASW, bistatic, multistatic, distributed surveillance, waveform diversity, Doppler detection, sensor placement, sensor management, multi-sensor data fusion, low frequency active sonar (LFAS)

1 Introduction

The multistatic sonar concept has been under evaluation at the NATO Undersea Research Center (NURC) for the past several years, for both LFAS and Deployable multistatic sonar configurations [1]. Multistatic fusion and tracking algorithms have been developed [2], and recently, these have been modified to accommodate bistatic Doppler information coming from a distributed surveillance network [3].

Multistatic sonar systems have the potential to greatly increase ASW performance. The geometric distribution of sonar sources and receivers provides a diversity of differing and complementary detection opportunities. The use of both Doppler-sensitive and Doppler-insensitive sonar waveform types within a geographically distributed multistatic system offers further diversity in target detection opportunities [4]. This detection diversity complicates the target's counter tactics. With multiple sources operating concurrently, it will be more difficult for targets to avoid providing good detection opportunities. This paper provides insights into sensor placement issues with waveform diversity for increasing target surveillance. Other sensor placement approaches to achieve cross-sensor localization benefits have also been developed [5].

2 Signal reverberation properties

In shallow water acoustic environments, reverberation is usually the dominant feature that obscures target detections. Reverberation rejection is a function of sonar waveform type. The reverberation at a sonar receiver is a function of the size and the scattering strength of the observed scattering patch. The time (or range) dimension of this patch is related to the time duration of the sonar pulse. The time resolution of the waveform at the output of the matched filter is determined by the signal's ambiguity function. Assuming a uniform distribution of dense scatterers throughout the area, the received reverberation is the sum of the received energy over the time dimension of the signal's ambiguity function. This is termed the Q-function, which depends on the characteristics of the sonar signal, and which measures the reduction in reverberation as a function of (target) Doppler search [6]. The Q-function can also be generalized to include the effects of frequency spread from a moving surface, but that effect is not considered here.

The Q-function is the integration over time of the waveform's ambiguity function. It is given as

$$Q(\Delta\upsilon) = 10\log_{10}\left[\int_{-T}^{T}\left|X(\Delta\upsilon,\tau)\right|^2 d\tau\right], \qquad (1)$$

where $|X|^2$ is the waveform's ambiguity function, T is the waveform's duration and $\Delta\upsilon$ is the Doppler shift of the target relative to the fixed reverberation field (in knots). The function is normalized such that its maximum (at zero Doppler) is set to zero.

Figures 1a and 1b show the well-known ambiguity functions for CW (f_c = 2000 Hz, T = 1 sec) and FM (f_c = 2000 Hz, T = 1 sec, W= 100 Hz) waveforms, respectively. The time resolution of the CW waveform is poor (~T), but quite good for the FM (~1/T). The Doppler resolution is good for the CW (~1/W), but poor for the FM.

Report Documentation Page

Form Approved
OMB No. 0704-0188

1. REPORT DATE	2. REPORT TYPE	3. DATES COVERED
JUL 2006		**00-00-2006 to 00-00-2006**

4. TITLE AND SUBTITLE	5a. CONTRACT NUMBER
Multi-sensor placement to exploit complementary properties of diverse sonar waveforms	5b. GRANT NUMBER
	5c. PROGRAM ELEMENT NUMBER
6. AUTHOR(S)	5d. PROJECT NUMBER
	5e. TASK NUMBER
	5f. WORK UNIT NUMBER
7. PERFORMING ORGANIZATION NAME(S) AND ADDRESS(ES) **NATO Undersea Research Center (NURC),Viale S. Bartolomeo 400,La Spezia, Italy, 19138,**	8. PERFORMING ORGANIZATION REPORT NUMBER
9. SPONSORING/MONITORING AGENCY NAME(S) AND ADDRESS(ES)	10. SPONSOR/MONITOR'S ACRONYM(S)
	11. SPONSOR/MONITOR'S REPORT NUMBER(S)

12. DISTRIBUTION/AVAILABILITY STATEMENT
Approved for public release; distribution unlimited

13. SUPPLEMENTARY NOTES
9th International Conference on Information Fusion, 10-13 July 2006, Florence, Italy. Sponsored by the International Society of Information Fusion (ISIF), Aerospace & Electronic Systems Society (AES), IEEE, ONR, ONR Global, Selex - Sistemi Integrati, Finmeccanica, BAE Systems, TNO, AFOSR's European Office of Aerospace Research and Development, and the NATO Undersea Research Centre. U.S. Government or Federal Rights License

14. ABSTRACT
see report

15. SUBJECT TERMS

16. SECURITY CLASSIFICATION OF:			17. LIMITATION OF ABSTRACT	18. NUMBER OF PAGES	19a. NAME OF RESPONSIBLE PERSON
a. REPORT **unclassified**	b. ABSTRACT **unclassified**	c. THIS PAGE **unclassified**	**Same as Report (SAR)**	**8**	

The Q-function is computed by integrating the ambiguity surface over the time dimension. Figure 2 shows the resulting Q-functions for the CW and FM waveforms, normalized so that the maximum (at zero Doppler) is 0 dB. These results show the effectiveness of the CW waveform in rejecting reverberation when the target search Doppler increases, but with little ability to reject reverberation near zero-Doppler. The FM shows moderate and nearly constant reverberation rejection over for all Doppler searches.

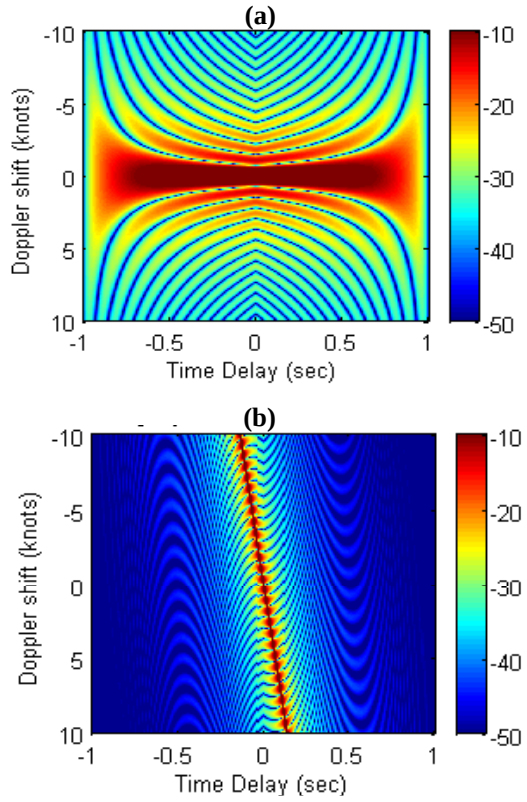

Figure 1. Signal ambiguity functions, (a) CW, (b) FM

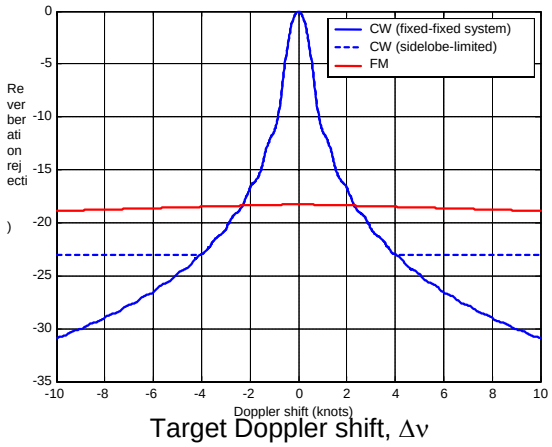

Figure 2. The Q-function for the CW and FM waveforms

In the case of sonar configurations where the source and/or receiver have motion, the Q-function for the CW is overly optimistic. A fixed sonar system will measure bottom reverberation from all ranges and azimuths as zero-Doppler. A mobile sonar system will measure the bottom reverberation with a range of apparent Doppler shifts induced by own system (source and/or receiver) motion. Because the beamforming process is unable to completely reject all the energy from non-steer directions, reverberation with various Doppler shifts will leak through the beam's sidelobes. Therefore, the capability of a moving system to reject reverberation using the CW waveform will in practice be limited by the sidelobe level of the array's beampattern. The dashed curve of figure 2 shows the effect on the CW's Q-function for array sidelobe level of -23 dB.

Comparing Q-functions for these signals, the CW waveform is more effective for Doppler searches greater than 2.5 knots. The amount of gain depends on target Doppler, and ranges from 0 dB at 2.5 knots to 12 dB at 10 knots Doppler shift. The FM waveform performs better for Doppler searches less than 2.5 knots, up to about 18 dB at zero-Doppler. The CW reverberation ridge will narrow as the pulse length or center frequency increases.

3 Bistatic Target Strength

The target strength (TS) of a submarine is aspect-dependent. Favorable angles will provide enhanced ability of the sonar to detect. One of the strengths of multistatic sonar is that there will be more opportunities within the geometry to experience these favorable aspect angles on the target. With multiple sources and receivers in a geometrically distributed layout, the threat target will have more difficulty denying such favorable aspects to some sor in the multistatic network.

Various models exist for bistatic target strength. The output of a simple but suitable TS model for an ensonified target is shown in figure 3. The vertical axis is given by the bistatic, or, opening angle (β), which is defined as the angle subtended by the source-target-receiver. The bistatic aspect angle (θ_{TB}) is defined as the angle between the target's heading and the bisector of the opening angle. The very strong "specular glint" condition is seen, at bistatic aspect angles of 90° or 270°. This occurs when there is symmetry of the source and receiver angles around the target's beam. There are additional TS enhancements near these specular conditions.

The model results also show very large target strength in the direction of extreme forward scatter (opening angles greater than 135°). Although the model predicts very high levels for this geometric condition, these cases correspond the target being within or very near to the direct blast-blanking zone, where detection is difficult due to high levels of received direct path acoustic energy. Therefore, the sensor placement and waveform selection schemes discussed in this paper do not attempt to exploit this TS feature.

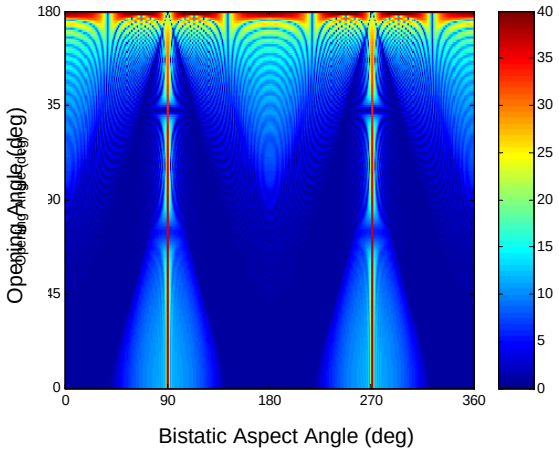

Figure 3. The bistatic target strength (TS), plotted as a function of opening (bistatic) angle, and bistatic aspect angle.

The bistatic geometry will therefore yield an enhancement in the target strength when the bistatic aspect angle is at or near 90° or 270°. This corresponds to the condition when the target's Doppler for that source-receiver node will be zero, as well be described later. In this situation detectability for CW waveforms will be low, and the use of FM waveforms is advised.

4 Bistatic Doppler

The difference in bistatic Doppler shift (in knots) between fixed scatterers (bottom reverberation) and a moving target is given by [7]

$$\Delta\upsilon = \left(\frac{1+\frac{V_R}{c}\cos\theta_{RT}}{1-\frac{V_S}{c}\cos\theta_{ST}} \right) \cdot V_T \cdot \cos\theta_{TB} \cdot \cos(\beta/2) \quad (2)$$

where, V_S, V_T, V_R, are the source, target and receiver speeds in knots, respectively, and θ_{RT} and θ_{ST} are the projection angles of source and receiver motion into their lines of bearing to the target, respectively. β is the bistatic or opening angle (angle formed between the source, target, and receiver), and θ_{TB} is the target's bistatic aspect angle (angle from the target's heading to the bisector of β).

In the special case of a geometry where both the source and receiver are in fixed positions, V_S = V_R = 0, we obtain

$$\Delta\upsilon_{FIX} = V_T \cdot \cos\theta_{TB} \cdot \cos(\beta/2) \quad (3)$$

The following observations can now be made:

- Bistatic Doppler is a function of the bistatic aspect and opening angles, which are also key parameters in describing Target Strength
- Whereas monostatic Doppler is only a function of bearing, Bistatic Doppler is a function of both bearing AND range
- Mobile systems may experience significant Doppler leakage from reverberation through beam's sidelobes, hence, fixed systems are best suited to exploit Doppler

5 Doppler and TS diversity

In this section we bring together the effects of the Q-function, bistatic target strength (TS) and bistatic Doppler, to show their complementary nature within a multistatic distributed field. Figure 4 shows a diagram of a bistatic source-receiver pair. Shown in blue are a set of confocal bistatic equi-time ellipses and an orthogonal set of hyperbolae for this source-receiver pair. The bistatic geometry is such that depending on the targets trajectory the following effects are simultaneously presented to the bistatic source-receiver node:

- In the case of motion tangential to the ellipses: a perfect specular "glint" condition where a large enhancement of target strength is expected, and a Doppler shift of zero (relative to fixed reverberation scatterers in the same target position). Here, frequency-modulated (FM) waveforms are expected to provide good detection capability because they are Doppler-insensitive.
- In the case of motion tangential to the hyperbolae: a range of Doppler shifts depending on the target's position relative to the foci, but for any particular position it will give the maximum possible target Doppler shift (relative to the reverberation), and, a relatively low target strength corresponding to a bow/stern orientation to the sonar (ignoring the region of blanking and extreme forward scattering). Pulsed continuous-wave (CW) waveforms are expected to provide good detection capability because they are Doppler-sensitive.

The actual Doppler provided by a target to the bistatic pair will almost always be less than its absolute speed depending on its location relative to the foci and its heading. As already seen, a target heading tangential to an ellipse will produce zero Doppler. The more a target's heading deviates from motion tangential to a hyperbola, the less Doppler shift it provides. Even when travelling tangentially along a hyperola the apparent Doppler will be reduced as the target approaches the blanking zone between the source and receiver. At the line between the source and receiver the Doppler falls to zero (β=180°). Figure 5 shows

the relevant Doppler scaling factor as function of source-target-receiver geometry.

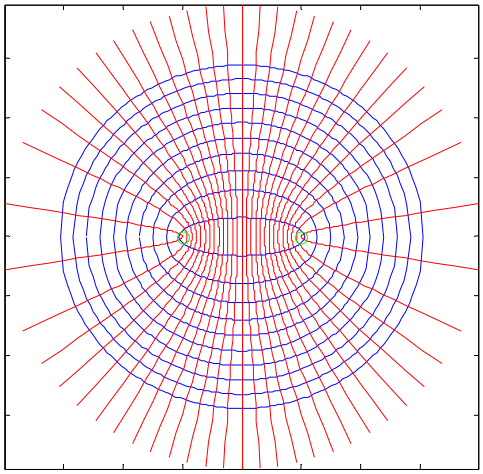

Figure 4. An orthogonal set of confocal equi-time ellipses and hyperbolae for a single bistatic source-receiver pair.

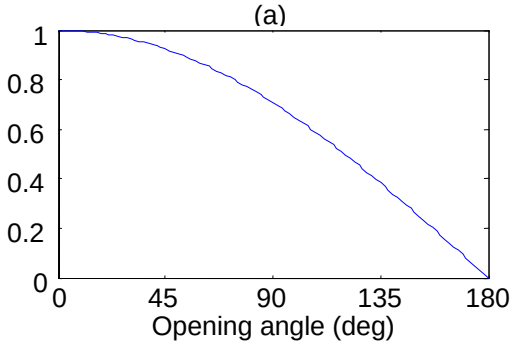

Figure 5. Fraction of target's absolute speed sensed as a Doppler shift (target travelling along hyperbola).

The relationship between the bistatic aspect angle (which is an indicator of the target strength) and the "delta" Doppler shift, $\Delta\upsilon$ (which is an indicator of detectability with CW waveforms) is shown in figure 6, for the monostatic case. As expected, good aspect angles (near 90°) correspond to zero Doppler, while poor aspect angles (with regard to target strength) correspond to high Doppler. Similar behavior is also seen for most of the observation cells of a bistatic pair, except when the target is penetrating between the source and receiver. In these cases the observable Doppler decreases, as described previously.

Since we know that CW waveforms will perform well for high target Doppler, and FM waveforms will perform well when specular angles are presented, it is important to know the distributions of detection opportunities as function of Doppler and bistatic aspect angle. A 25 square nmi surveillance box is considered, with a centrally located bistatic source and receiver (5 nmi separation). A uniform grid of 10,000 surveillance cells are considered as potential target locations, and for each cell, 9 possible target headings (evenly spaced over 360°) are assumed. Figure 7 shows the histograms of all target detection opportunities (a total of 90,000) versus Doppler and bistatic aspect angle.

These histograms show that statistically, there will be more opportunities to detect high Doppler targets than low Doppler targets. This is an important result because it gives further incentive to utilize Doppler sensitive waveforms within fixed-fixed multistatic fields. The shape of this distribution is consistent with that of a sinusoid function, indicating that most of the detection opportunities are occurring according to the monostatic Doppler relationship (which is simply the cosine of the aspect angle, as shown in previously). The distribution for bistatic aspect angle is uniform, and consistent with the equal probability of (evenly spaced) target headings that were assumed.

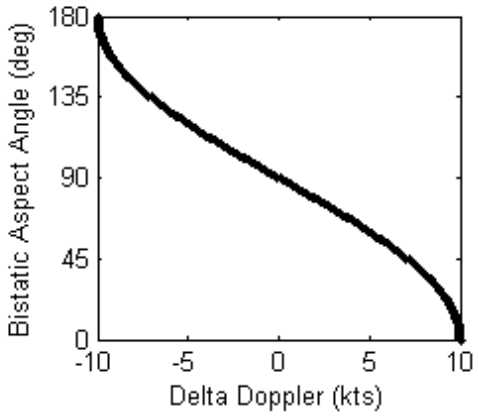

Figure 6. Scatter plot of detection opportunities.

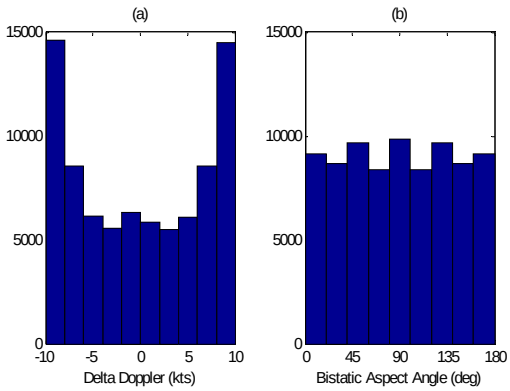

Figure 7. Histograms of detection opportunities as a function of (a) Doppler, (b) bistatic aspect angle.

Using the monostatic relationship between the bistatic aspect angle and Doppler, we can visualize the complementary nature of the CW and FM waveforms. Figure 8a overlays the target strength (monostatic) and the gain in reverberation rejection according to

the Q-function, on the same dB scale versus the target's aspect angle. The specular "glint" feature of the target strength is seen as a very sharp narrow peak at 90°, with an enhanced region of target strength around it. The red curves show the Q-function performance for both the CW (solid line) and the FM (dashed line). We see that the Q-function for the CW performs well at high Doppler, but has a hole in performance precisely where the target strength is high. By summing the Q-function gain and the target strength, we can directly compare the performance of the two waveforms, as seen in figure 8b. We see that the highest strength echoes will be made by a source-receiver pair situated to achieve the "glint" when using an FM waveform. The use of the CW gives more modest echo levels, but provides more robust surveillance coverage over wide range of possible geometries.

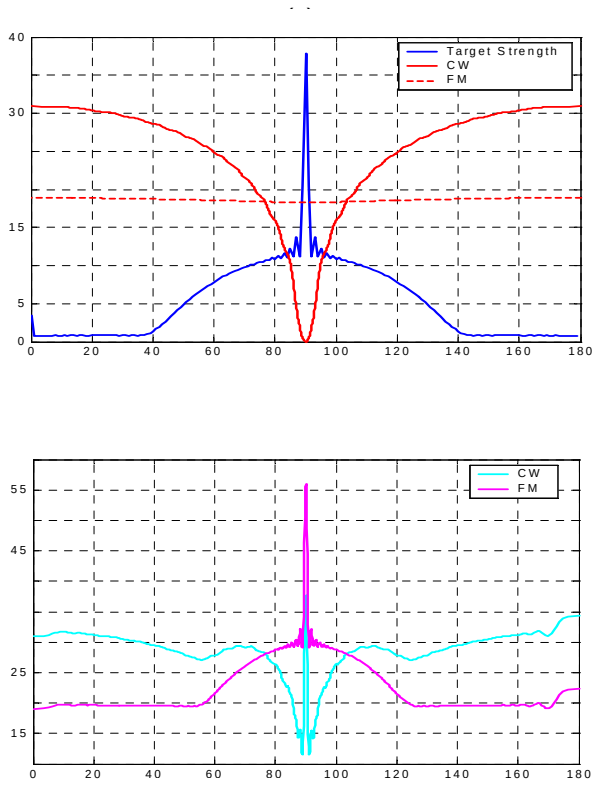

Figure 8. (a) TS and Q functions overlaid on common dB scale. (b) Sum of TS and Q functions.

So far we have considered only a single bistatic source-reciever node. Now we consider the advantages of the combined use of geometric and waveform diversity. Figure 9 shows two sets of confocal equi-time ellipses for two different bistatic nodal pairs in red and blue. Two boxes showing regions of interest are highlighted. In the left region, we observe that the inter-nodal ellipses are nearly parallel. A target moving in this area will present nearly the same type of detection opportunity to each of the two nodes, either low Doppler (target moving tangential to ellipses) or high Doppler (target moving orthogonal to ellipses), or some combination. This region therefore does not have a large amount of inter-nodal geometric diversity, and whichever of the two waveforms best detects for one node, it will also detect best for the other. In the upper region we observe a large amount of orthogonality between the ellipses of the two nodes. In such a region, if the target is traveling tangentially to one set of ellipses (with high target strength but zero target Doppler), it is simultaneously presenting high Doppler to the other node, and vice versa. This zone has a large amount of geometric diversity, and the choice of waveforms on each node may differ to exploit their particular geometric detection opportunities.

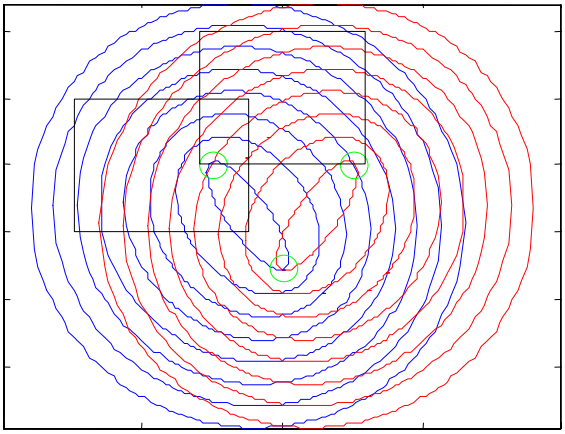

Figure 9. Two sets of confocal ellipses with regions of low(left) and high (upper) inter-nodal diversity.

6 Simplified Signal Excess Modeling

To compare performance based on signal excess, we must consider the modeling of the bistatic sonar equation. Some simplifying assumptions in the modeling are made, in order to focus only on the multistatic waveform and placement diversity effects. The bistatic sonar equation for a reverberation-limited active sonar is given as

$$SE = EL - RL - DT \tag{4}$$

where SE is the signal excess in dB above a detection threshold DT. EL is the target's echo level against a reverberation background level RL, as given by

$$\begin{aligned} EL &= SL - TL_{ST} - TL_{TR} + TS \\ RL &= SL - TL_{SP} - TL_{PR} + BTS \end{aligned} \tag{5}$$

where SL is the transmitter's source level, TL_{ST} and TL_{SP} are the transmission losses from the source to target and the reverberation patch, TL_{TR} and TL_{PR} are the transmission losses from the target and the reverberation patch to the receiver, TS is the target strength, and BTS is the bottom target strength.

We assume here, for the purposes of this simplified model, that propagation losses are similar for the target and the ensonified reverberation patch beneath it. This approximation can be justifiably made in many shallow water environments. Making this assumption (i.e., $TL_{ST} = TL_{SP}$, and $TL_{TR} = TL_{TP}$), we obtain

$$SE = TS - BTS - DT \tag{6}$$

Therefore, for a given receive array and fixed detection threshold, detectability increases through increases in target strength and decreases in the bottom target strength. The bottom target strength is a function of the bottom scattering strength SS (dB/area), the sonar's ensonified patch area, and the waveforms reverberation rejection properties (Q-function). The sonar equation then becomes

$$SE = TS - SS - 10\log_{10}\left(\frac{c \cdot R_{RP} \cdot \Omega \cdot B(\gamma)}{2}\right) - Q(\Delta\upsilon) - DT \tag{7}$$

where R_{RP} is the range from the receiver to the patch, Ω is the beamwidth (in radians), and $B(\gamma)$ is a factor (normally between x and x) that corrects the patch length for the case of a bistatic geometry [xx]. $B(\gamma)$ = 1, in the case of a monostatic sonar. $Q(\nu)$ is the (normalized or negative-valued) Q-function, which reduces the amount of reverberation energy as a function of the target's Doppler shift, as previously described. For a Doppler insensitive waveform the Q-function becomes $10\log_{10}(1/W)$, where W is the signals bandwidth. Comparing performance between waveforms on a one or more different source-receiver waveform using this modeling approach are now be made.

7 Signal Excess Comparisons

In this section, we utilize the signal excess model described in the previous section to gain insight into the diversity and complementariness of multiple sensor placement and waveforms. This is done first for scenarios with a single source-receiver node and later for multiple nodes.

The modeled area is a 25x25 nmi box, divided into 10,000 grid cells. Each grid cell in the box corresponds to a potential location of the target, which is moving with a user-specified heading and speed (in this case 10 knots). Sources are designated by the circle symbols and receivers are designated by the square symbols, and are assumed "fixed" systems. The target's Target Strength (TS) is calculated according the model previously shown. Each source has the possibility to transmit both CW and FM waveforms. The assumed Q-functions for the CW and FM signals are those previously calculated. Both waveforms have duration of 1 second and a center frequency of 2 kHz. The FM signal has a bandwidth of 100 Hz. The bottom scattering strength is assumed tobe –43 dB globally, which corresponds to McKenzie scattering with an average grazing angle of 9°. The detection threshold (DT) is 10 dB for all receivers, which are assumed to be bottom reverberation-limited for all observation cells in the area. The receiver beamwidths are all assumed to be 8°, consistent with the capability of the NURC's DEMUS surveillance system.

We begin by assuming a single source, placed at the center of the surveillance box (0,0), with one receiver to the north (node 1) and one receiver to the east (node 2), each spaced at 5 nmi from the source. Figure 10 shows the modeled Signal Excess, for a potential target at each grid cell, with heading of 135° T, for the two nodes and both waveform types. The CW waveform gives good signal excess (as shown in green/yellow) spread out over a large area, except to the northeast and southwest, where the target Doppler is zero (shown in blue). The FM waveform gives very high values of signal excess (shown in red) precisely in the region where the CW gives poor values of signal excess due to the "specular glint". However, the FM's performance is much poorer in the regions where target Doppler is high. In both cases, the signal excess is higher on the receiver side of the bistatic pair, because the reverberation patches are smaller near the receiver (hence lower reverberation levels).

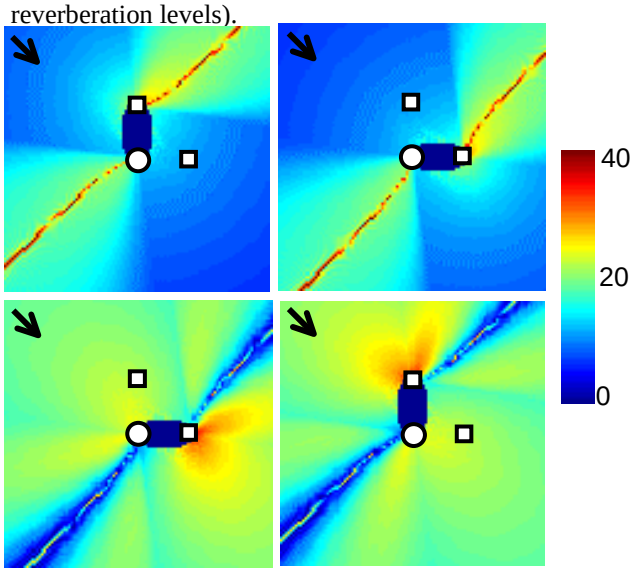

Figure 10. Modeled signal excess maps. (a) Node1 - FM, (b) Node2 - FM, (c) Node1 -CW, (d) Node2 -CW.

Now we consider the fusion of the results obtained with a single node and single waveform type. The fusion applied is an "OR" fusion, wherein the maximum signal excess of the various fusion inputs is taken. In figure 11 the "combined" signal excess maps are shown for various combinations. We see the improved signal excess coverage, compared to a single node. Each fused image combines the best performance of the individual components, whether they be specular glint zones or Doppler zones.

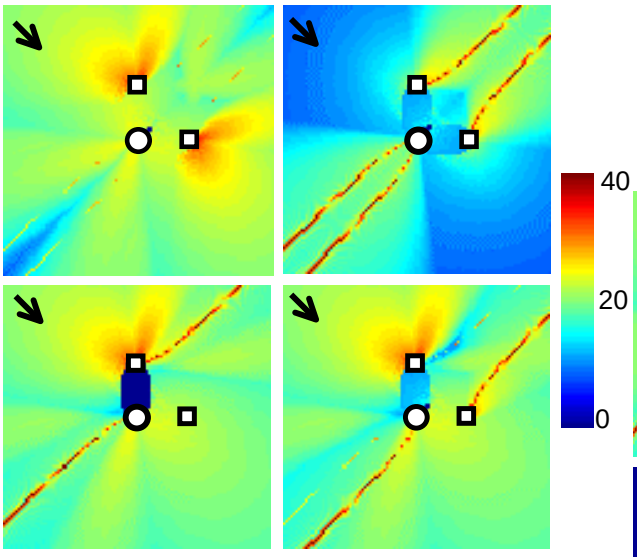

Figure 11. 2-node fusion (a) CW Node1-Node2 (b) FM Node1-Node2 (c) Node1 CW-FM (d) Node2 CW-FM.

Figure 12a shows the results of combining both nodes (1 and 2) and both waveform types (CW and FM). Here, not surprisingly, we achieve the best signal excess coverage over the whole region. We observe see the contributions of the two Doppler zones and the two specular zones. Figure 12b shows the fused signal excess obtained when the source is replaced by a receiver and the receivers are replaced by sources. The areas of high signal excess, whether they be the specular glints or the Doppler zones, are seen to move to the receiver side (now to the southwest) of the bistatic pairs. Figures 12c and 12d show color-coded segmentation maps, indicating the areas for which the four individual fusion components provided the highest signal excess in the fusion process (navy- node1 CW; yellow- node2 CW; cyan- node1 FM; and brown- node2 FM). From this we see that most of the area (from a percentage point of view) is best covered through the use of CW waveforms, rather than the FM waveforms. The FM waveforms provide a much higher value of SE, but over a more limited area.

So far we have only considered a target traveling with a heading of 135° T. Figure 13 shows the results of full fusion when the target is assumed to be travelling with different headings. Notice how the specular "trip wires" rotate and the high Doppler zones shift.

Now a more complex case is considered, with a field composed of 4 sources and 4 receivers. One source and receiver are assumed to be collocated, in the center of the area, in a monostatic configuration. Three other receivers and sources are positioned at a range of 5 nmi alternately spaced in angle every 60 degrees. The receivers are located at bearings of 0°, 120°, and 240° T, relative to the centered system. The sources are located at bearings of 60°, 180°, and 300° T. With 4 sources and 4 receivers, there are a total of 16 bistatic detection nodes in the multistatic network. Each source can transmit both CW and FM waveforms, which will yield 32 possible detection opportunities. The target is assumed to travel with a heading of 135° T.

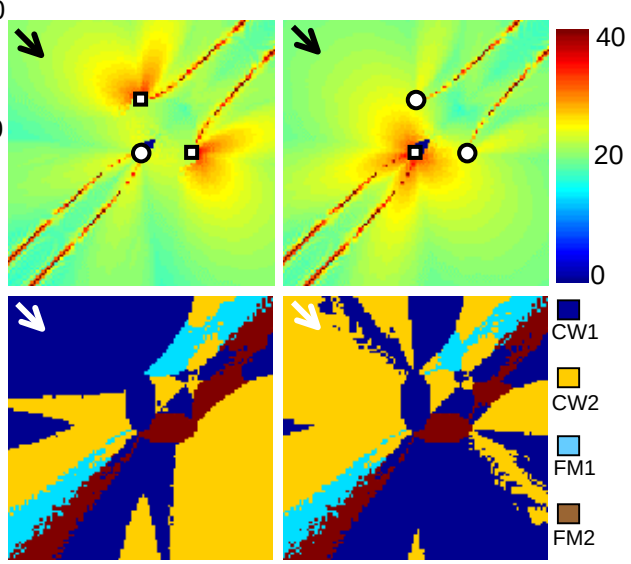

Figure 12. Full fusion and segmentation maps, (a,c) 1 source, 2 receivers, (b,d) 2 sources, 1 receivers.

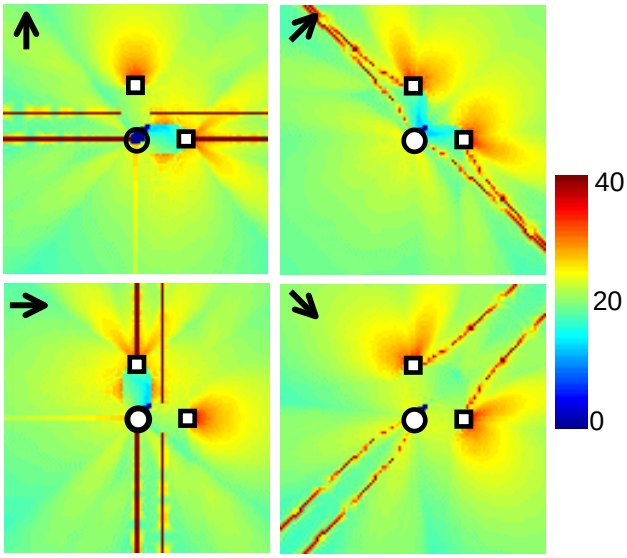

Figure 13. Full fusion with various target headings (a) 0°T, (b) 45°T, (c) 90°T, (d) 135°T.

Figure 14 shows the modeling results for both waveforms types with a single node (panels a and b), and fusion with all nodes for either the CW or FM waveform (panels c and d). The CW fusion of all nodes has raised the signal excess significantly within and around the field. The FM fusion shows an increased number (sixteen) of the specular glint zones within and extending from the field. The total fusion of all nodes and both waveforms (32 cases) are shown

in the figure 15. The performance of the network over the whole area has considerably improved.

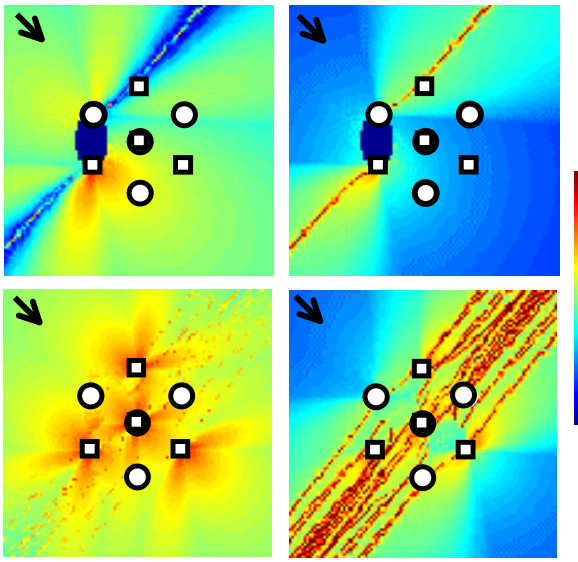

Figure 14. 16 node field. (a) west node CW, (b) west node FM, (c) all nodes CW, (d) all nodes FM..

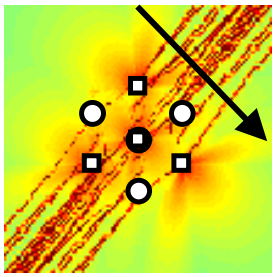

Figure 15. 16 node field, full fusion.

Figure 16 shows the overlaid signal excess for each node along a hypothetical target trajectory (heading 135° T, speed of 10 knots), as show overlaid in black in figure 15. The trajectory passes by to the northeast of the field. CW cases are shown in red and FM cases are shown in blue. The diversity of performance is evident. The CW cases provide better coverage when the target approaches and leave the field. The high-level specular glint opportunities are evident. The duration of time spent within a glint condition varies by node. There are also opportunities with good simultaneous CW and FM coverage by different nodes. Any deep gaps between specular opportunities are covered well by the nodes using the CW.

8 Conclusions

The analysis and modeling results show the presence of areas of extremely high SE for FM waveforms when there is a specular condition, for each node within the network. These opportunities, however, are constrained to quite limited geographic areas. The use of the CW provides better wide area coverage, although with more moderate SE levels. The simultaneous use of both of these waveform types within the deployed field will provide complimentary and diverse detection opportunities. Such operations will increase target vulnerability and reduce its tactical options for remaining undetected and a robust surveillance capability. Using these modeling approaches and sensor placement concepts, a well-designed field placement pattern can be obtained to provide a more robust detection capability.

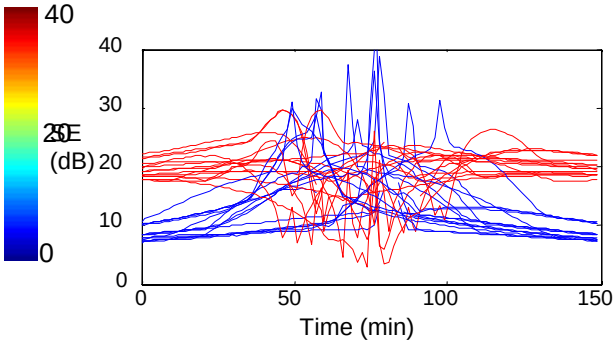

Figure 16. Nodal SE over time of trajectory.

References

[1] S. Jespers and D. Grimmett, Data association and interoperability of Multi-static LFAS platforms, in *Proceedings of the RTO SCI Panel Symposium SCI-116,* October, 2002, Norfolk VA, USA.

[2] S. Coraluppi and D. Grimmett, Multistatic Sonar Tracking, in *Proceedings of the SPIE Conference on Signal Processing, Sensor Fusion, and Target Recognition XII*, April 2003, Orlando, FL, USA.

[3] Coraluppi, S., Grimmett, D., Gerard, O., Distributed Multi-Hypothesis Tracking and Extensions, *NURC Technical Report SR-421*, 2004.

[4] D. Grimmett, Multistatic sensor placement with the complementary use of Doppler sensitive and insensitive waveforms, *NURC Report SR-427*, July 2005.

[5] D. Grimmett and S. Coraluppi, Sensitivity Analysis for Multistatic LFAS Localization Accuracy, *NURC Report SR-386*, January 2004.

[6] M. Brill, X. Zabal, M. Harman, and A. Eller, Doppler-Based Detection in Reverberation-Limited Channels: Effects of Surface Motion and Signal Spectrum, *OCEANS'93 'Engineering in Harmony with Ocean', Proceedings IEEE*, 1993 Vol 1, pp 1220-1224, 1993.

[7] H. Cox, Fundamentals of Bistatic Active Sonar, in *Underwater Acoustic Data Processing*, Kluwer Academic Publishers, 1989.